Revista Brasileira de Geografia Física v.18, n.03 (2025) 1697-1713.

Revista Brasileira de Geografia Física

ISSN:1984-2295

Homepage:https://periodicos.ufpe.br/revistas/rbgfe

Impacts of the Great May 2024 Geomagnetic Storm on Precise Point Positioning

William Rodrigo Dal Poz, professor da Universidade Federal de Viçosa, MG. william.dalpoz@ufv.br, Alex Carvalho Silva, aluno da Universidade Federal de Viçosa, MG. alex.c.silva@ufv.br, Afonso de Paula dos Santos, professor da Universidade Federal de Viçosa, MG. afonso.santos@ufv.br, Nilcilene das Graças Medeiros, professora da Universidade Federal de Viçosa, MG. nilcilene.medeiros@ufv.br, Ítalo Oliveira Ferreira, professor da Universidade Federal de Viçosa, MG. italo.ferreira@ufv.br Júlio Cesar de Oliveira, Universidade Federal de Viçosa. oliveirajc@ufv.br

Artigo recebido em 23/05/2024 e aceito em 24/01/2025

R E S U M O

Efeitos adversos do clima espacial podem ser uma das principais ameaças à tecnologia humana, como por exemplo, efeitos decorrentes de grandes ejeções de massa coronal. Consequentemente, grandes tempestades geomagnéticas podem comprometer a performance do Posicionamento por Ponto Preciso (PPP). Recentemente, após mais de duas décadas, no dia 10/05/2024, teve início a fase principal de uma grande e excepcional tempestade. Trata-se, portanto, de uma grande e singular oportunidade para estudar seus efeitos no PPP, com uso do serviço online CSRS-PPP. Este trabalho tem como objetivo avaliar os impactos da grande tempestade nas acurácias tridimensionais, porcentagem de solução das ambiguidades e perdas de ciclos, englobando cinco dias de processamento, contemplando 2 dias antes da tempestade, 1 dia coincidente com a fase principal da tempestade e 2 dias após a tempestade, coincidente com a fase de recuperação. Os processamentos foram realizados com intervalo de 1 hora, das 23-24 UTC, coincidente com parte do período da fase principal, visto que os efeitos adversos da tempestade se manifestam nesta fase. Foram utilizados dados de 20 estações GNSS da Rede Brasileira de Monitoramento Contínuo dos Sistemas GNSS, mantida pelo IBGE. Durante a fase principal da tempestade, a acuraria tridimensional média aumentou em torno 4 vezes em relação ao dia anterior. A porcentagem da solução das ambiguidades foi igual a 0.0 % para todas as estações analisadas. Além disso, as perdas de ciclos aumentaram significativamente durante a fase principal da tempestade. Em síntese, os resultados obtidos evidenciam os impactos adversos da grande e excepcional tempestade no PPP.

Palavras-chave: Tempestade geomagnética, Posicionamento por Ponto Preciso, GNSS, Ionosfera.

Impactos da grande tempestade geomagnética de 2024 no Posicionamento por Ponto Preciso

ABSTRACT

The adverse effects of space weather can be one of the main threats to human technology, such as the effects of large coronal mass ejections. Consequently, great geomagnetic storms can compromise the performance of Precise Point Positioning (PPP). Recently, after over two decades, on 05/10/2024, the main phase of a great and exceptional geomagnetic storm began, providing an excellent and rare opportunity to study its effects on the PPP using the CSRS-PPP online service. This work aims to evaluate the impacts of the great storm on three-dimensional accuracies, percentage of ambiguity resolution, and cycle slip, encompassing five days of processing, covering two days before the storm, one day coinciding with the main phase of the storm, and two days after the storm, coinciding with the recovery phase. The processing was carried out at an interval of 1 hour, from 23-24 UTC, coinciding with the main phase (05/10/2024), as the adverse effects of the storm manifest themselves in this phase. Data from 20 GNSS stations from the Brazilian Network for Continuous Monitoring of GNSS Systems were used. During the main phase of the storm, the average three-dimensional accuracy increased around four times compared to the previous day. The percentage of ambiguity resolution was equal to 0.0% for all stations analyzed. Furthermore, cycle slips increased significantly during the main phase of the storm. In summary, the results highlight the adverse impacts of the great and exceptional storm on the PPP.

Keywords: Geomagnetic storm, Precise Point Positioning, GNSS, Ionosphere.

Introduction

Adverse space weather is one of the principal threats to modern human technology. Solar coronal mass ejections, large solar flares, and high-speed solar wind streams often lead to sequences of damaging disturbances within the Earth's magnetosphere, in the atmosphere, and even on the Earth's surface. Powerful and long-lasting geomagnetic storms can develop following solar disturbances (Baker, 2005).

Geomagnetic Storms have the potential to affect Global Navigation Satellite System (GNSS) signals, which can seriously impact the navigation and positioning performance of GNSS (Luo et al., 2022; Wang et al., 2023). Storms are typically classified as weak, moderate, strong, severe, and great storms (Loewe and Prölss, 1997). These classifications are determined based on indexes such as Planetary K (Kp) and Disturbance Storm Time (Dst).

The Kp is a three-hour geomagnetic disturbance index that describes the general state of geomagnetic activity. It is a scale from 0 (quiet) to 9 (disturbed) (Moldwin, 2022). It is an important measure of the energy input from the solar wind to Earth, and space weather services use it in near real-time. The German Research Centre for Geosciences (GFZ) provides Kp (GFZ, 2024).

According to the National Oceanic and Atmospheric Administration (NOAA) Space Weather Scales, geomagnetic storms have numbered levels (G scale) from 0 to 5. A Kp index 9 means an extreme geomagnetic storm (G=5) (NOAA, 2024a).

The Dst index measures the deviation (in nano Teslas - nT) or changes in Earth's magnetic field from its average quiet time value, the strength of Earth's internal magnetic field (Moldwin, 2022). Selected magnetometer measurements are combined to determine the Dst index to provide an average measure of the magnetic disturbance (Otto, 2005). It is a geomagnetic index that measures the magnitude of geomagnetic storms. The Dst index has a standard behavior (signature) during geomagnetic storm events.

The principal characteristic of a geomagnetic storm is the so-called "main phase," i.e., the interval of a significant decrease in Dst (Gonzalez et al., 1994). The Dst index can drop by several 100 nT (negative values) within a few hours. After the main phase, there is a second phase of a slow (days) recovery (recovery phase) of the Dst (Otto, 2005) until it reaches approximately the quiet value, which occurs when there is no storm. The energy input to the upper atmosphere is maximized during the main phase, while during the recovery phase, the geomagnetic activity and energy input decrease (Schunk and Nagy, 2009).

However, there is no unique definition of the strength of the geomagnetic storms concerning the Dst index, as the thresholds differ between different authors (Miteva and Samwel, 2023).

This research will adopt the classification proposed by Loewe and Prölss (1997). This classification considers great storms with a Dst index below -350 nT. These events are considered exceptional, as in the recent May 2024 storm (05/10/2024). This storm was similar to historic storms in 1958 and 2003 (NASA, 2024), reaching a peak Dst of -351 nT on 05/10/24 at 23-24 UTC (WDC, 2024).

Storms (main phase) are usually associated with increased electron densities in the lower ionosphere (Komjathy, 1997). During the main phase, the ionosphere's electron density can show high variation rates (Yasyukevich et al., 2020). Furthermore, it can increase the occurrence of irregularities in the ionosphere and ionospheric scintillation effects. A phenomenon of weakening TEC intensity occurs mainly during the recovery phase of geomagnetic storms (Wang et al., 2023). However, disturbance remained in the early storm recovery phase (Wan et al., 2021).

Ionospheric scintillations are rapid random fluctuations in the amplitude and phase of electromagnetic wave signals observed by a radio receiver. They happen when the signals pass through irregularities in the electron density distribution of the ionosphere. Scintillation affects radio wave propagation, including GNSS signals (Imam et al., 2024). Therefore, signal loss or cycle slip may occur due to the weakening of the signal received by the GNSS receivers, adversely affecting the performance of the GNSS positioning, including Precise Point Positioning (PPP) (Caldeira et al., 2020). In this event, the integer counter is reinitialized, which causes a jump in the instantaneous accumulated phase by an integer number of cycles. This jump is called a cycle slip, which is restricted to phase measurements (Hofmann et al., 2008). A cycle slip is a momentary disruption of phase tracking (Beeck et al., 2023).

From a global perspective, ionospheric scintillation is most prominent at equatorial and low latitudes (Zheng et al., 2022), particularly around the geomagnetic equator after local sunset (GPS WORLD, 2024).

PPP can achieve decimeter or even millimeter levels of positioning accuracy in general. However, this accuracy will be degraded significantly under a strong geomagnetic storm, which is a major disturbance of Earth's magnetosphere that occurs when there is a very efficient exchange of energy from the solar wind into the space environment surrounding Earth (Luo et al., 2022).

Although PPP has definite advantages for many applications, its merits and widespread adoption are limited by the convergence time. The convergence time is defined as the time required for the position or ambiguity estimates to reach a specific level of accuracy and does not deviate beyond this level after reaching it (Choy et al., 2017). Therefore, the PPP accuracy can be decreased due to the subsequent reconvergence caused by frequent cycle slips during geomagnetic storms (Lu et al., 2020).

Several online PPP services exist, including the Canadian Spatial Reference System Precise Point Positioning (CSRS-PPP). The Canadian Geodetic Survey (CGS) of Natural Resources Canada (NRCan) updated the CSRS-PPP service on Tuesday, 20 October 2020, including the PPP with Ambiguity Resolution (PPP-AR) (NRCAN, 2024a).

Various studies have been carried out to evaluate the impact of storms on GNSS positioning, such as Berdermann et al. (2018), Odolinski and Teunissen (2019), Filjar (2021), and Zhow et al. (2024). Luo et al. (2018, 2022a, 2022b, and 2023), Lu et al. (2020), Alcay (2022), Paziewski et al. (2022), Mou et al. (2023), and Wang et al. (2023) assessed the impacts of storms on the PPP.

However, due to the recent event in 2024 and its exceptional nature, no articles have yet been published considering its effects on the PPP.

This research aims to evaluate the impacts of the great geomagnetic storm of 2024 on CSRS-PPP (NRCAN, 2024b) in Brazilian territory, covering part of the equatorial and low-latitude regions. For this, Brazil has the Brazilian Network for Continuous Monitoring of the GNSS Systems (RBMC), which provides free GNSS data distributed throughout Brazilian territory. The study aims to assess the effects of the great storm on three-dimensional accuracy, percentage of ambiguity resolution, and cycle slip.

Great geomagnetic storms are exceptional events, like the one that occurred in 2024 after over two decades (since 2003). As highlighted by the director of the Space Weather Prediction Center of the National Oceanic and Atmospheric Administration (NOAA), considering the great storm of 2024, he states, "*This is an unusual and potentially historic event*" (NOAA, 2024b). The space weather conditions that led to the great storm will be detailed in the following sequence.

Material and methods

The great geomagnetic storm of 2024 May

On 05/09/2024, multiple Coronal Mass Ejections ("MCE Cannibal") were recorded towards Earth (Space Weather, 2024). NOAA space weather forecasters have observed at least seven CMEs from the sun (NOAA, 2024b). The dominant interplanetary phenomena causing intense magnetic storms are the interplanetary manifestations of fast CME (Gonzalez et al., 1999).

On 05/10/2024, the solar wind speed reached 725.1 km/s; on 05/11/2024, it reached 907.2 km/s. On calm days, solar wind speeds are typically between 300 and 400 kilometers per second. This information was obtained from the website www.spaceweather.com. As the Kp index indicates, this space weather condition has caused an extreme storm (Figure 1).

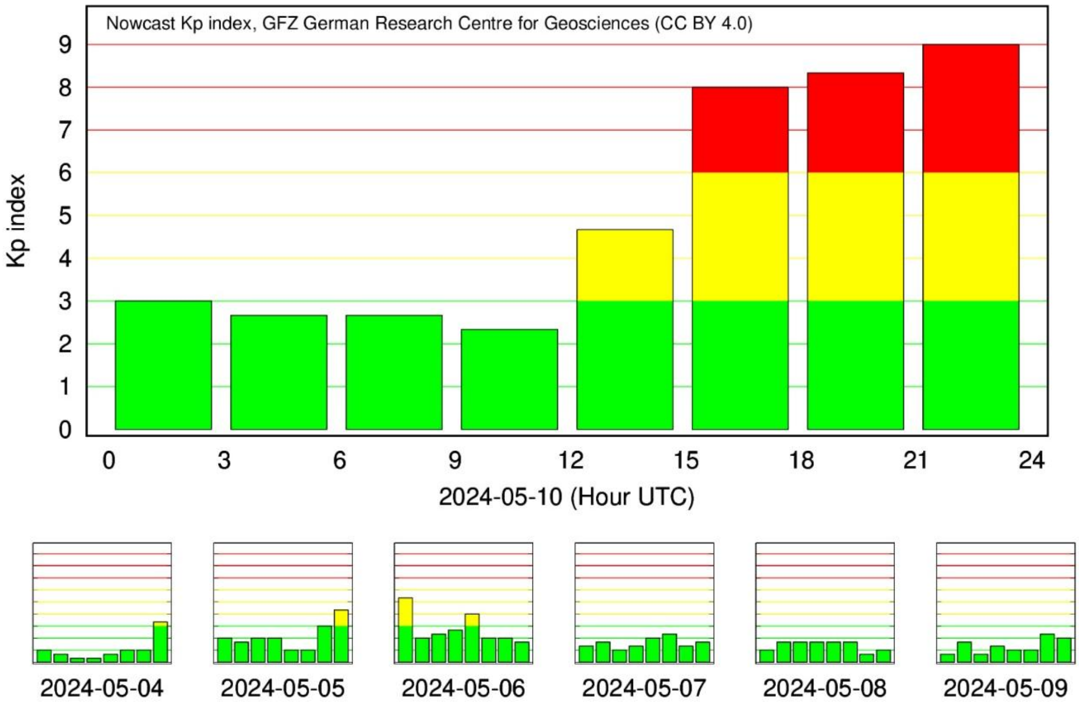

Figure 1. Kp index for 2024-05-10.
Source: https://kp.gfz-potsdam.de/en/hp30-hp60/daily-plots

Based on the information from Figure 1, the kp index has reached a value of 9 (21 – 24 UTC), categorizing the storm as extreme.

Figure 2 illustrates the Dst index for May 2024.

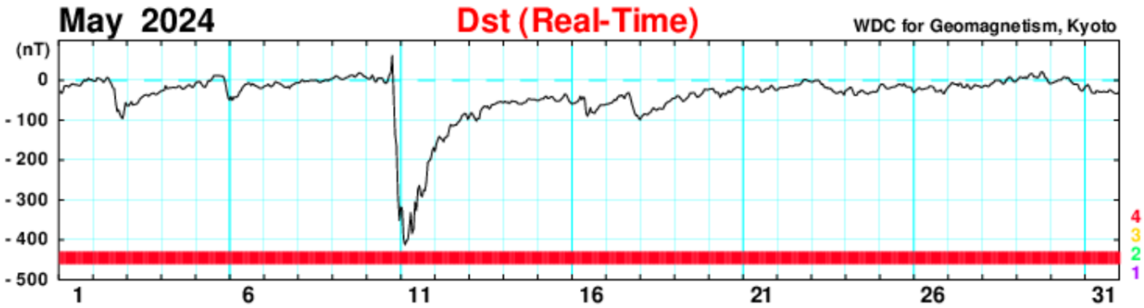

Figure 2. Dst index for May 2024.
Source: https://wdc.kugi.kyoto-u.ac.jp/dst_realtime/202405/index.html

According to Figure 2, the main phase of the storm began on 05/10/2024 (23-24 UTC), reaching a peak Dst of -351 nT (great storm). During this period, the storm is expected to have the most significant impact on GNSS positioning. The storm recovery phase began on 05/11/2024.

Data GNSS processing

The study used data from 20 RBMC GNSS stations, as shown in Figure 3. The data, in Receiver Independent Exchange Format (RINEX v2.11), includes GPS and GLONASS observations. GNSS data was collected over five days, including two days before, one day during the storm (05/10/2024 – main phase), and two days after. GNSS data was processed during the main phase of the storm, from 23 to 24 UTC (05/10/2024).

In this manner, 100 values (20 stations x 5 days) of three-dimensional accuracies, 100 values of percentages of ambiguity solutions, and cycle slips have been obtained.

In CSRS-PPP, ambiguity resolution is performed on the backward run. This means that epochs are first processed chronologically to ensure all information is available before resolving ambiguities. Starting with the last epoch successfully processed, then, beginning with the last epoch successfully processed, ambiguity resolution is attempted.

This process is repeated for all epochs in reverse order (from last to first epoch) (NRCAN, 2020). In CSRS-PPP, GLONASS ambiguities are not resolved.

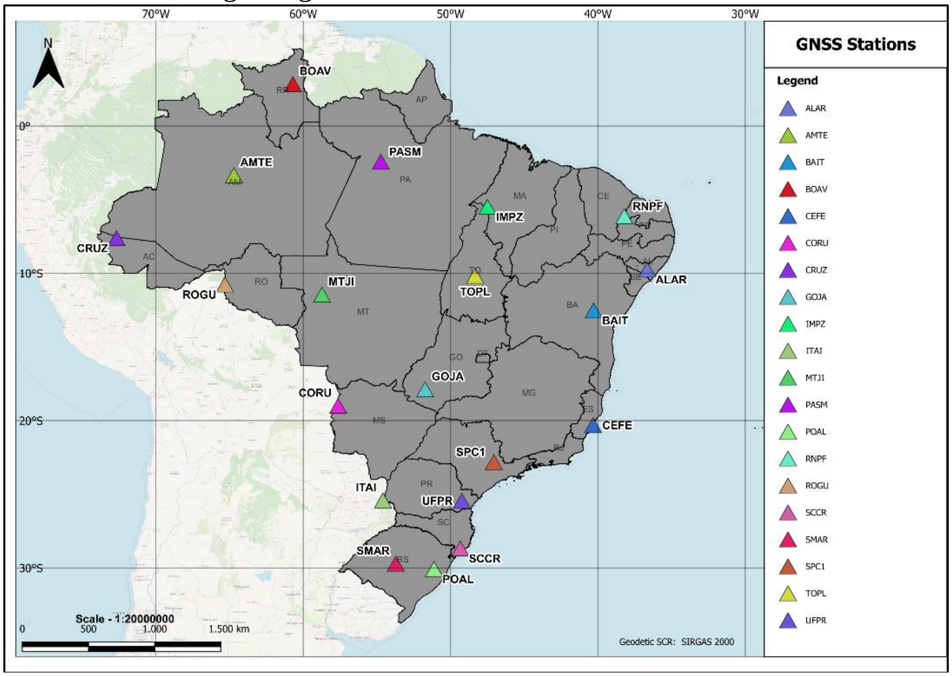

Figure 3. Spatial distribution of GNSS stations in Brazil.

The standard deviations from CSRS-PPP with 95% significance in Cartesian components (σx, σy, σz) are used to calculate three-dimensional precisions (TDP) using Equation 1.

$$TDP = \sqrt{\sigma x^2 + \sigma y^2 + \sigma z^2} \quad (1)$$

An error is the difference between a measured value for any quantity and its true value In theory, the true value of a quantity can never be determined (Ghilani, 2018). However, in practice, a reference value is typically designated as true. Based on this, the three-dimensional discrepancies (“error”) (TDD) were calculated by comparing the estimated coordinates with the reference coordinates of the RBMC stations, at the same epoch and frame from the CSRS-PPP estimated coordinates using Equations 2, 3, 4, and 5.

$$\mathrm{dX} = \mathrm{Xe} - \mathrm{Xr} \quad (2)$$

$$\mathrm{dY} = \mathrm{Ye} - \mathrm{Yr} \quad (3)$$

$$\mathrm{dZ} = \mathrm{Ze} - \mathrm{Zr} \quad (4)$$

$$\mathrm{TDD} = \sqrt{\mathrm{dX}^2 + \mathrm{dY}^2 + \mathrm{dZ}^2} \quad (5)$$

Were,

Xe, Ye, Ze: three-dimensional estimated coordinates in Earth-Centred, Earth-Fixed (ECEF).

Xr, Yr, Zr: three-dimensional reference coordinates in ECEF.

Beginning with GNSS observations collected on Sunday, 27 November 2022, CSRS-PPP will output ITRF solutions in the IGS20 reference frame. This new frame is the International GNSS Service (IGS) realization of ITRF2020 (NRCAN, 2024b).

The reference coordinates were obtained from weekly positions generated by DGFI-TUM for the SIRGAS stations from RBMC, in the same epoch and frame (IGS20) as the estimated coordinates in CSRS-PPP (SIRGAS, 2024), to reduce the effect of displacement of the South American tectonic plate over time. The operational SIRGAS weekly solutions refer to the IGS reference frame valid at the time (IGS20) when the analysis of GNSS data is made. This enables a rigorous analysis of the results.

We will assess the results using three-dimensional accuracy (TDA) calculated by Equation 6.

$$\mathrm{TDA} = \sqrt{\mathrm{TDP}^2 + \mathrm{TDD}^2} \qquad (6)$$

Equation 6 includes both random and systematic (bias) effects (Monico et al., 2009).

The ambiguity resolution percentages and cycle slips available in the processing reports were also evaluated from heatmap charts using MATLAB version 2022b (academic use).

Results and Discussion

The 3D accuracies (TDA) for the 20 RBMC stations are depicted in Figures 4, 5, 6, and 7. Graphs indicate the conventional Day-Of-Year (DOY) calendar form, which is widely used in GNSS. The DOYs 129 to 133 represent, respectively, the dates 05/08/24 to 05/12/24. Due to the absence of GNSS data from the AMTE station for DOY 132, no accuracy value is presented in the figure (blank space in Figure 4). The highest TDA value occurred during the main phase of the storm (DOY 131 – Figure 4) at AMTE station (0.607 m). The lowest TDA value was 0.048 m for the CORU (DOY 129 – Figure 5) two days before the storm.

In the two days before the storm, the maximum TDA value was 0.277 m for the CRUZ station (DOY 129 – Figure 5). In contrast, as previously mentioned, on the day of the main phase of the storm, the highest value was 0.607 m for the AMTE station (DOY 131 – Figure 4), representing an increase of around two times the maximum value obtained before the storm. During the main phase of the storm (DOY 131), there were no TDA values recorded at the centimeter level (< 0.10 m).

On DOY 129, there were 15 occurrences of TDA at the centimeter level, followed by 16 occurrences on DOY 130 (before the storm). Post-storm (DOY 132), seven occurrences of centimeter-level TDA values were recorded, and 14 two days later (DOY 133).

After the main phase, the highest 3D accuracy value (0.326 m) occurred at the SMAR station (DOY 132 – Figure 6), while the lowest value reached 0.052 m for the IMPZ station (DOY 132 – Figure 5).

Only three stations (ITAI - Figure 5, SMAR - Figure 6, and SPC1 – Figure 7) did not provide the highest TDA values in the main phase of the storm. In this case, the highest values occurred on the first day of the recovery phase of the storm (DOY 132).

On DOY 129, the average TDA value was 0.099 m; on DOY 130, it was 0.086 m; on the day of the storm (main phase—DOY 131), it increased to 0.339 m. In the storm recovery phase, on DOY 132, the precision value decreased by 0.157 m; on DOY 133, it decreased to 0.112 m.

In the initial recovery phase (DOY 132), ionospheric disturbances may still occur, given that the average precision value (0.157 m) is almost twice that of the day preceding the storm (0.086m). During the recovery phase of the geomagnetic storm, ionospheric disturbances may persist (Wang et al., 2023).

He et al. (2023) also highlighted these conclusions. In this study, the positioning error anomalies are mainly concentrated in the main phase and early recovery phase of the geomagnetic storms. The percentages of ambiguity solutions for each RBMC station and their average values for the five days are depicted in the heatmap chart (Figure 8). Tones of darker blue indicate higher percentages. In legend, “NaN” denotes the absence of GNSS data for the AMTE station on DOY 132 from 23 – 24 UTC.

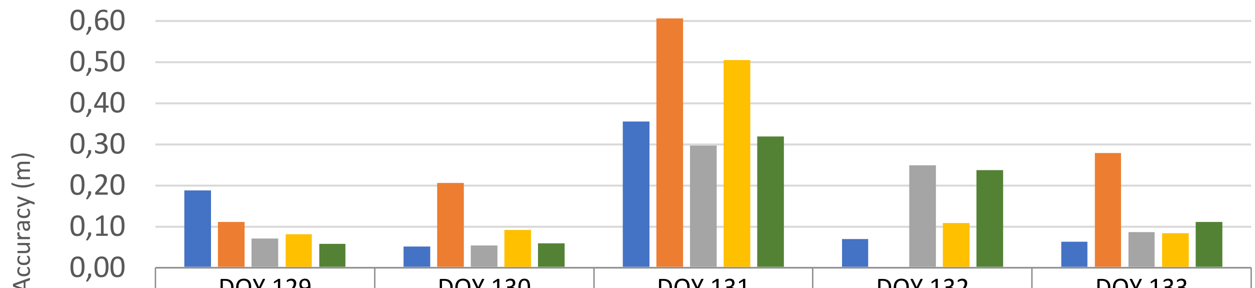

	DOY 129	DOY 130	DOY 131	DOY 132	DOY 133
ALAR	0,187	0,052	0,356	0,070	0,063
AMTE	0,111	0,207	0,607		0,280
BAIT	0,071	0,055	0,298	0,249	0,087
BOAV	0,082	0,092	0,505	0,109	0,084
CEFE	0,058	0,060	0,319	0,237	0,111

Figure 4 – 3D accuracy of RBMC stations (ALAR, AMTE, BAIT, BOAV, CEFE)

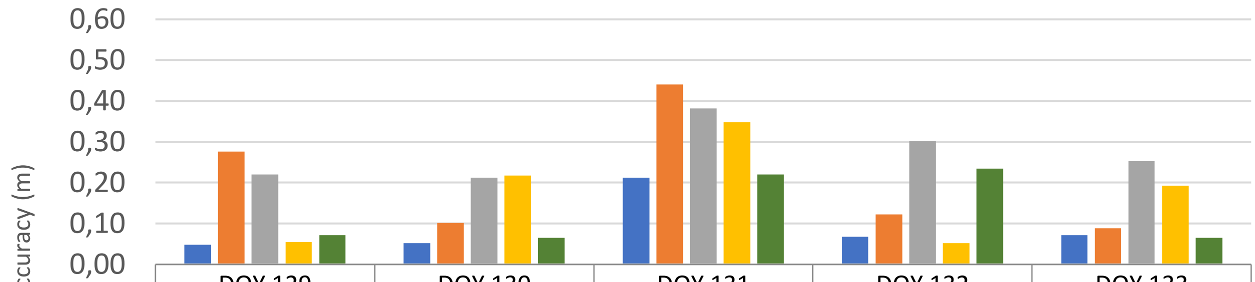

	DOY 129	DOY 130	DOY 131	DOY 132	DOY 133
CORU	0,048	0,052	0,213	0,067	0,072
CRUZ	0,277	0,102	0,441	0,122	0,088
GOJA	0,220	0,212	0,382	0,303	0,252
IMPZ	0,055	0,218	0,348	0,052	0,193
ITAI	0,072	0,065	0,220	0,235	0,066

Figure 5 – 3D accuracy of RBMC stations (CORU, CRUZ, GOJA, IMPZ, ITAI)

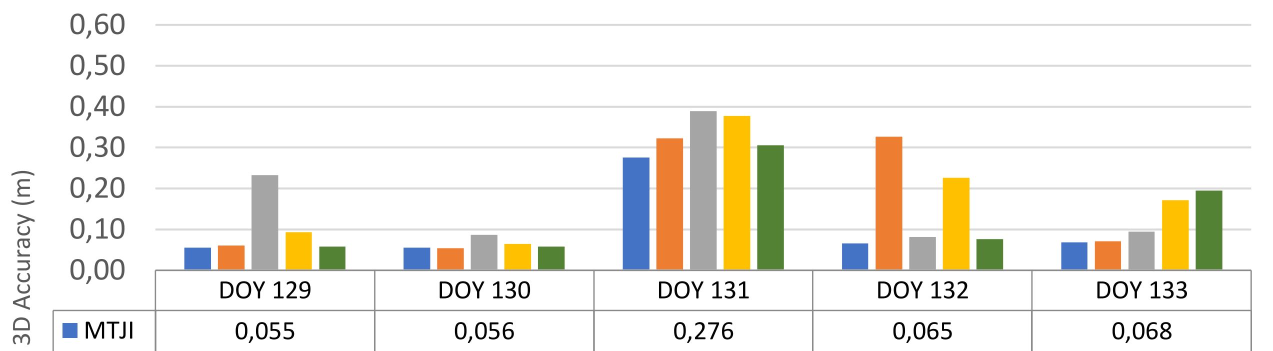

	DOY 129	DOY 130	DOY 131	DOY 132	DOY 133
MTJI	0,055	0,056	0,276	0,065	0,068
SMAR	0,061	0,054	0,323	0,326	0,071
PASM	0,233	0,086	0,389	0,082	0,095
POAL	0,093	0,064	0,377	0,226	0,171
RNPF	0,058	0,057	0,306	0,076	0,195

Figure 6 – 3D accuracy of RBMC stations (MTJI, SMAR, PASM, POAL, RNPF)

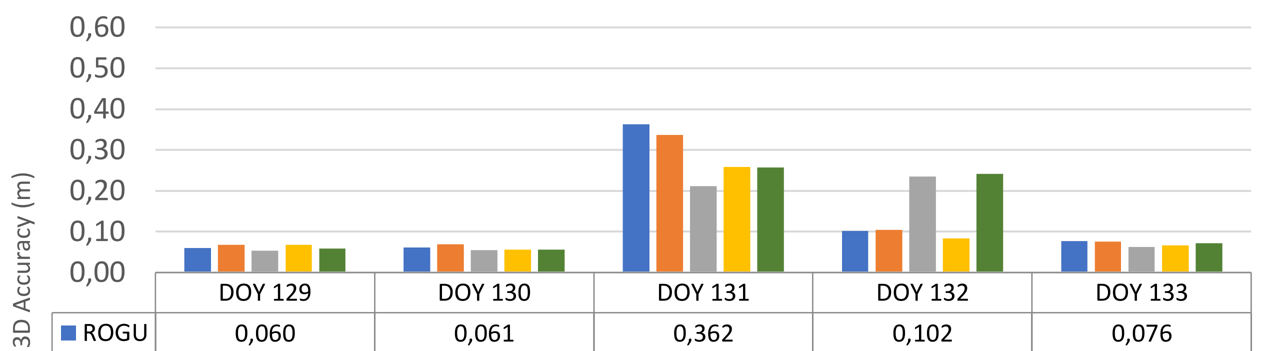

	DOY 129	DOY 130	DOY 131	DOY 132	DOY 133
ROGU	0,060	0,061	0,362	0,102	0,076
SCCR	0,068	0,069	0,337	0,105	0,076
SPC1	0,053	0,055	0,212	0,235	0,063
TOPL	0,068	0,056	0,259	0,083	0,067
UFPR	0,059	0,056	0,257	0,241	0,071

Figure 7 – 3D accuracy of RBMC stations (ROGU, SCCR, SPC1, TOPL, UFPR)

On DOY 129, the average ambiguity resolution percentage was about 55%, increasing to around 69% on DOY 130. However, on the day of the storm (DOY 131), the average dropped to 0%, indicating the significant impact of the main phase in GNSS signals. After the main phase, the average increased to 31% (DOY 132) and approximately 48% on DOY 133. Throughout the main phase of the storm, the percentages of ambiguity solutions consistently registered 0%, as identified in Figure 8 (middle of heatmap chart).

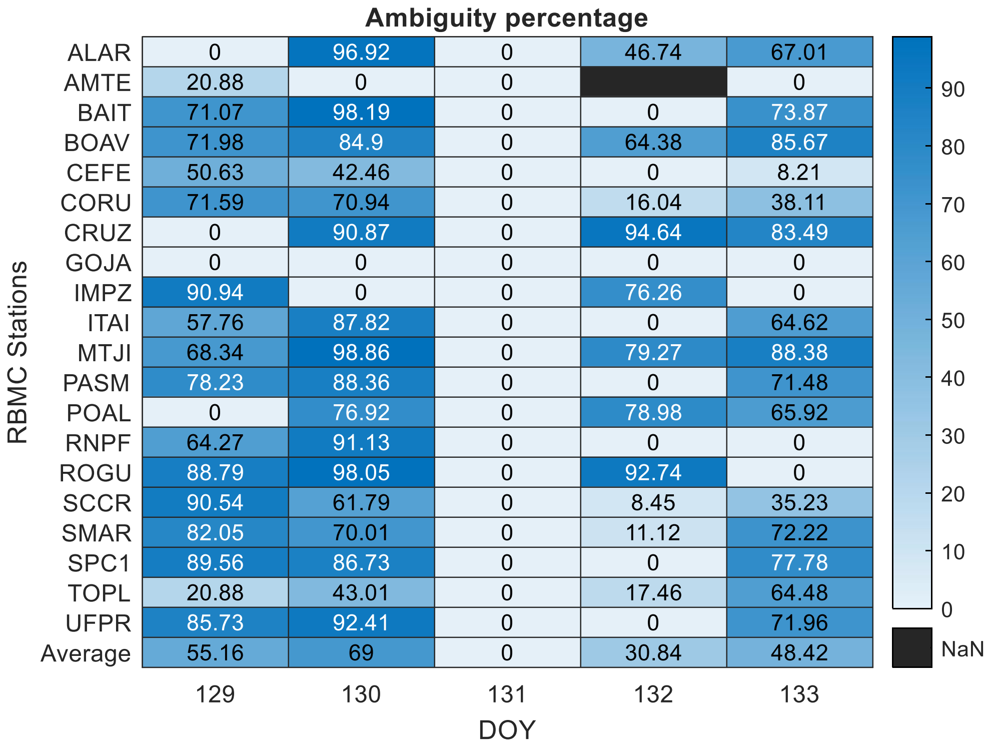

Figure 8 – Ambiguity percentage.

Figure 8 also shows the storm's impact on the first day of the recovery phase (DOY 132). On this day, the average ambiguity resolution percentage was still very low at 31%. Only six stations had values greater than 50%. Additionally, the ambiguity resolution percentages at eight stations were equal to 0.0%.

As stated in the introduction, storm effects can significantly increase the density and variation in electron density in the ionosphere, negatively impacting positioning performance. Furthermore, ionospheric scintillation effects may occur. As a result, cycle slips may happen in the GNSS signals, contaminating the data and resulting in very short arcs. In this case, the CSRS-PPP could not confidently resolve ambiguities and provided a float solution (NRCAN, 2020).

The mechanism for the decrease in ambiguity resolution percentage under geomagnetic storms is mainly due to the cycle slips of GNSS signals caused by storm-induced ionospheric disturbances and scintillations (Luo et al., 2023).

To analyze the impact of the main phase of the storm in cycle slips, the station BOAV will be taken as an example, which delivered low accuracy during the main phase of the storm (0.505 m). The processing report indicates that 84.9% of ambiguities were resolved as integers one day before the storm (Figure 8 – DOY 130).

The Ambiguity Status Plot (ASP) for the observation session of station BOAV (23-24 UTC), one day before the storm, is shown in Figure 9. Since no attempt has been made to resolve GLONASS ambiguities, the figure illustrates only the satellites of the GPS constellation.

Firstly, we can note that GPS signals were collected from 11 satellites. The ASP illustrates the status of estimated ambiguities for all satellites at each epoch. The green color indicates when the ambiguity has been resolved as integers (fixed solution in 84.9%). The olive color indicates float ambiguity (satellites G06 and G25).

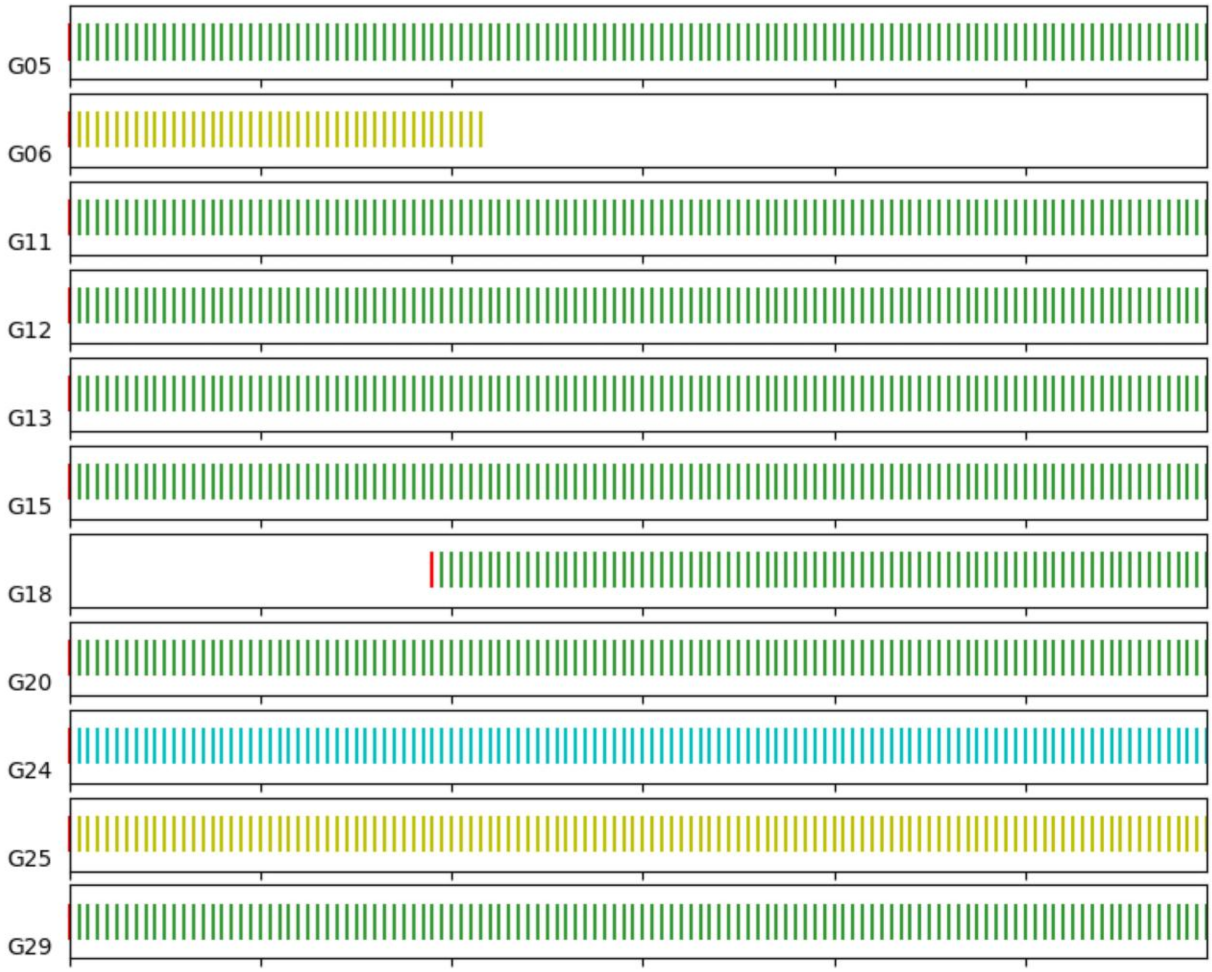

Figure 9 – Ambiguity status for BOAV station – (DOY 130)

The cyan color indicates "datum ambiguity," according to Collins et al. (2010). Red indicates a new ambiguity (arc). The vertical red lines in satellite G18 indicate cycle slip. Due to the high percentage of integer ambiguities on the day before the storm (DOY 130 – Figure 8), the three-dimensional accuracy was equal to 0.092 m, which is very close to the average value (0.086 m) before the storm.

On the day of the storm, the three-dimensional accuracy increased to 0.505 m, with the percentage of integer ambiguities at 0.0%, demonstrating the adverse impacts of the great storm. Figure 10 shows the ASP on the day of the storm (DOY 131 – main phase) for the station BOAV. The figure shows a very different scenario from the day before the storm. In this case, all solutions were float. The plot shows a high occurrence of cycle slip (red), which resulted in very short arcs (olive) and ambiguity resets.

As mentioned in the introduction, cycle slips may arise from ionospheric scintillation and great storms, adversely affecting the performance of the GNSS positioning due to the successive reconvergence that consistently occurs in the main phase of the storm.

Figure 10 – Ambiguity status for BOAV station – (DOY 131)

One day after the main phase of the storm (DOY 132), the ambiguity resolution percentage increased to 64.38%; the following day (DOY 133), it increased to 85.67% (Figure 8).

Before the storm, a high 3D accuracy value of around 0.28 m was observed at CRUZ station (see Figure 5 - DOY 129). However, the occurrence of cycle slips was significantly lower (Figure 11) than the day of the storm, as shown in Figure 12 (DOY 131). Both figures illustrate the ASP for the observation session of station CRUZ (23-24 UTC).

Based on the data in Figure 11, there were two cycle slips for satellite G18, contributing to a total of 9 cycle slips. The CRUZ station receiver observed nine satellites, two less than the BOAV station. This is due to the fact that the equatorial region (BOAV – Figure 3) provides a greater number of satellites.

The data in Figure 12 (DOY 131 – CRUZ station) indicates that the number of cycle slips significantly increased on the day of the storm. A critical factor limiting the adoption of PPP in many applications is the convergence time needed to reach centimeter-level accuracies (Banville et al., 2021). Hence, cycle slips play a crucial role in PPP accuracy because of the repeated periods of reconvergence. In the main phase of the storm, it was impossible to reach centimeter-level accuracies. It is important to note that with a GPS-only solution, the positioning accuracy can be better than 1 dm after a convergence time of about 30 minutes (Li et al., 2015).

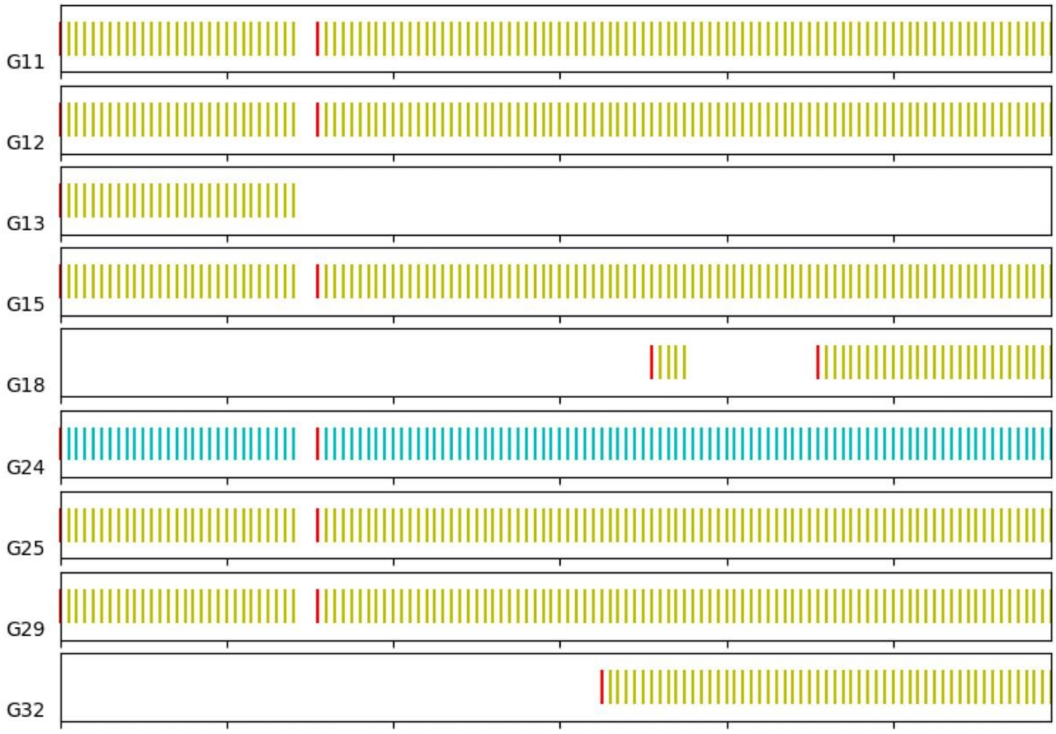

Figure 11 – Ambiguity status for CRUZ station – (DOY 129)

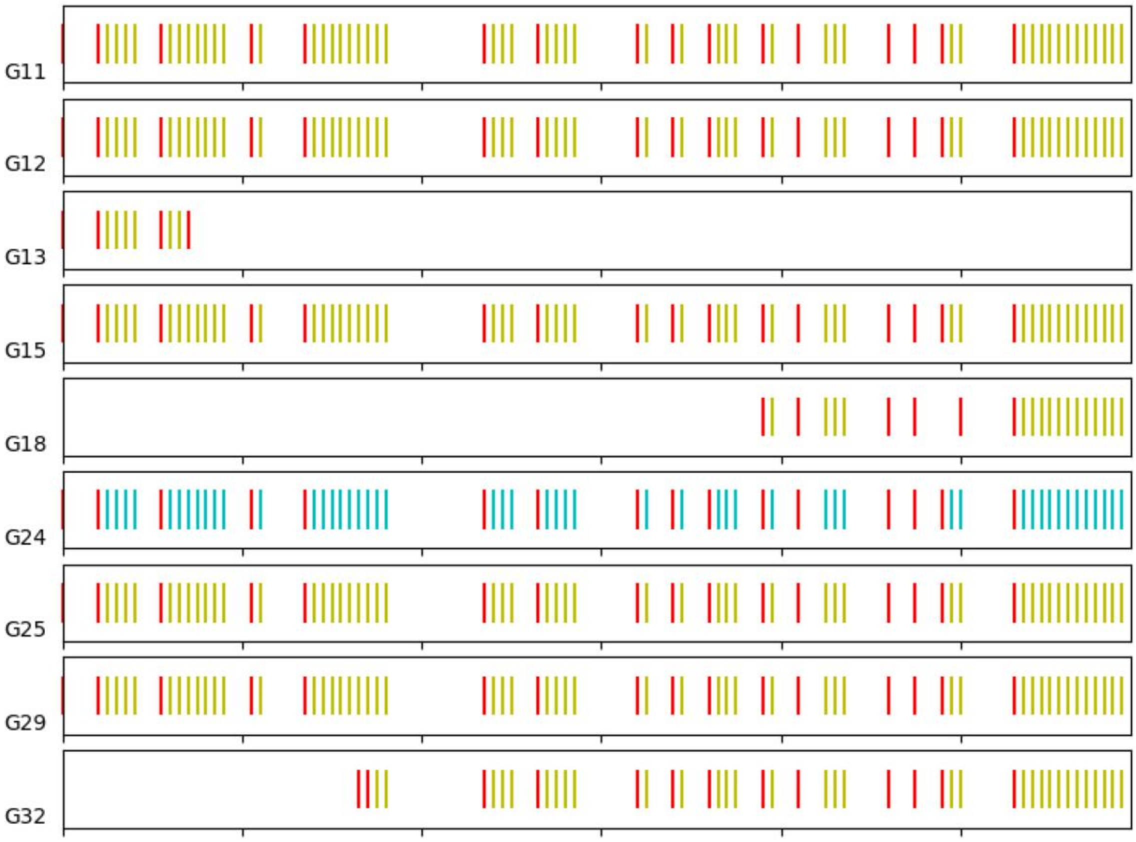

Figure 12 – Ambiguity status for CRUZ station – (DOY 131)

The cycle slips for each RBMC station and their average value for the five days are depicted in Figure 13 (heatmap chart). On DOY 129, the average cycle slips were about 14, which decreased to around five on DOY 130. However, on the day of the storm (DOY 131), average cycle slips increased to around 141, indicating the adverse impact of the main phase in GNSS signals. After the main phase, the average decreased to around 13 (DOY 132) and increased to 18 on DOY 133.

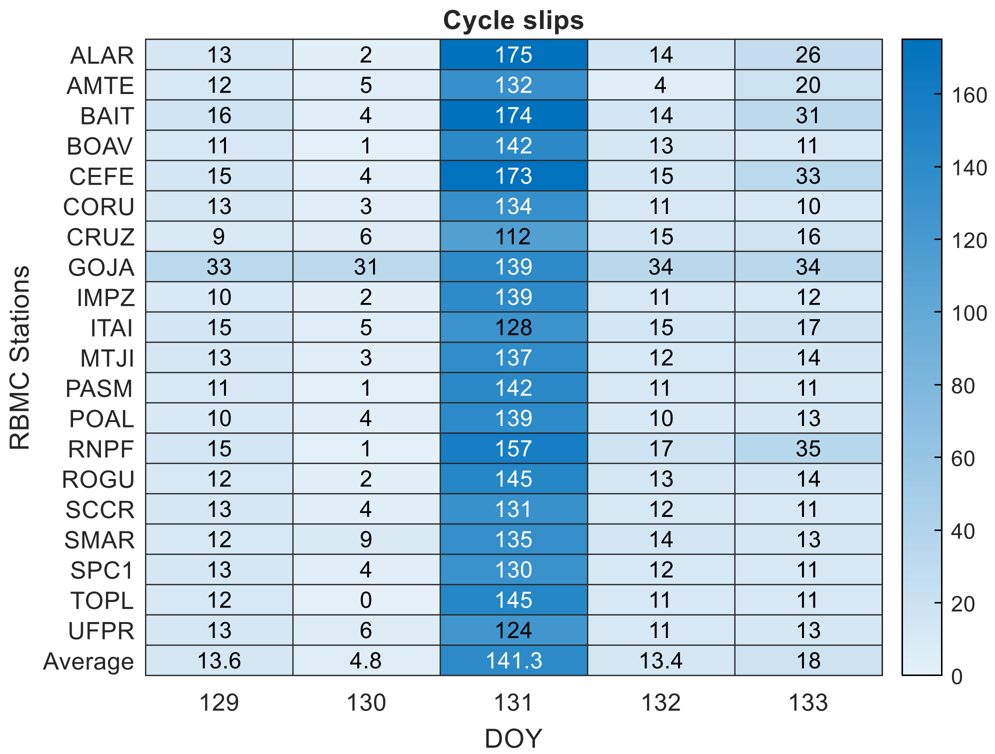

Figure 13 – Cycle Slips

It is essential to highlight that the lowest average value of TDA occurred on the day before the storm (0.086 m) on DOY 130. The lowest cycle slip values also occurred on DOY 130. For instance, at the TOPL station, no cycle slip occurred. The GOJA station presented a different behavior from the other stations. The days before and after the storm resulted in high cycle slips exceeding 30. According to the processing reports, this station led to several epochs where the satellite was rejected (missing observations). This may be related to receiver tracking issues. In addition, the GOJA station consistently maintained an ambiguity percentage of 0.0% (Figure 8).

In all cases with accuracy values exceeding 0.015 m, the ambiguity resolution percentages were 0.0%.

Given the results obtained, the impact of the main phase of the storm on the percentage of solution of ambiguities and cycle slips is evident, implying the adverse performance of the CSRS-PPP due to the increase in three-dimensional accuracies.

Conclusion

This study used GNSS data from RBMC to investigate the effects of the great geomagnetic storm of 2024 on PPP.

The study used data from 20 RBMC GNSS stations distributed throughout Brazilian territory. GNSS data was collected over five days, including two days before, one day during the storm (main phase), and two days after. GNSS data processing was carried out during the 23-24 UTC period, aligning with the main phase of the storm.

Three-dimensional accuracies were evaluated, as well as the percentages of ambiguity resolutions and cycle slips. Major conclusions can be summarized as follows:

1. The main phase of the storm had a significant adverse impact on the CSRS-PPP, leading to a remarkable increase in the average three-dimensional accuracy to 0.339 m. This represents an increase of around four times compared to the day before the storm (0.086 m).
2. During the early stages of recovery, it's important to note that ionospheric disturbances may continue to occur. This is indicated by the average accuracy value (0.157 m), which is nearly double that of the day before the storm (0.086m).
3. Due to the main phase effects, the percentage of ambiguity solutions decreased to 0.0% for all GNSS stations.
4. During the main phase, cycle slips increased significantly. Hence, cycle slips play a crucial role in PPP accuracy because of the repeated periods of reconvergence. In the main phase of the storm, it was impossible to reach centimeter-level accuracies.

We have presented the main conclusions here. It is important to note that events of this magnitude, such as the storm analyzed, are rare and exceptional. Therefore, future research should analyze GNSS data from globally distributed stations, such as those provided by the IGS network.

Acknowledgments

The authors would like to thank the Brazilian Network for Continuous Monitoring of the GNSS Systems (RBMC-IBGE) for providing GNSS data, the Canadian Geodetic Survey (CGS) of Natural Resources Canada (NRCan) for granting access to their online service CSRS-PPP, the Helmholtz Centre Potsdam German Research Centre for Geosciences GFZ for providing the Kp index and the World Data Center for Geomagnetism, Kyoto, for providing the Dst index.

References

Alcay, S. (2022) Ionospheric response to extreme events and its effects on precise point positioning. *Indian Journal of Physics*. 96, 3721–3734. https://doi.org/10.1007/s12648-022-02343-x.

Baker, D. N. (2005) *Introduction to Space Weather*. In: Scherer, K., Fichtner, H., Heber, B., Mall, U. (Eds.), Space Weather, Lect. Notes Phys. 656 (Springer, Berlin Heidelberg).

Banville S, Hassen E, Lamothe P, Farinaccio J, Donahue B, Mireault Y, Goudarzi MA, Collins P, Ghoddousi-Fard R, Kamali O. (2021) Enabling ambiguity resolution in CSRS-PPP. *NAVIGATION*. *68*(2):433–451. https://doi.org/10.1002/navi.423.

Beeck, S. S., Mitchell, C. N., Jensen, A. B. O., Stenseng, L., Pinto Jayawardena, T., Olesen, D. H. (2023). Experimental Determination of the Ionospheric Effects and Cycle Slip Phenomena for Galileo and GPS in the Arctic. *Remote Sensing*, *15(24)*, 5685. https://doi.org/10.3390/rs15245685.

Berdermann, J., Kriegel, M., Bany´s, D., Heymann, F., Hoque, M. M., Wilken, V. (2018). Ionospheric response to the X9.3 Flare on 6 September 2017 and its implication for navigation services over Europe. *Space Weather*, 16, 1604–1615. https://doi.org/10.1029/2018SW001933.

Caldeira, M. C. O.; Caldeira, C. R. T.; Cereja S. S. A.; Alves, D. B. M.; Aguiar, C. R. (2020) Evaluation of the GNSS positioning performance under influence of the ionospheric scintillation. *Bulletin of Geodetic Sciences*. 26(3). https://doi.org/10.1590/s1982-21702020000300014.

Choy, S., Bisnath, S. & Rizos, C. (2017) Uncovering common misconceptions in GNSS Precise Point Positioning and its future prospect. *GPS Solutions* 21, 13–22. https://doi.org/10.1007/s10291-016-0545-x.

Collins, P., Bisnath, S., Lahaye, F., Héroux, P. (2010) Undifferenced GPS Ambiguity Resolution using the Decoupled Clock Model and Ambiguity Datum Fixing. *Journal of the Institute of Navigation*, v.57, n.2, p. 123-135. https://doi.org/10.1002/j.2161-4296.2010.tb01772.x.

Filjar, R. (2021) *A Contribution to Short-Term Rapidly Developing Geomagnetic Storm Classification for GNSS Ionosphere Effects*

Mitigation Model Development. Seventh International Conference on Aerospace Science and Engineering (ICASE 2021), Islamabad, Pakistan, 1-6, doi:10.1109/ICASE54940.2021.9904168.

GFZ (Geo Forschungs Zentrum). (2024, May 30). Geomagnetic Kp index. https://kp.gfz-potsdam.de/en/.

Ghilani, C. D. (2018) Adjustment Computations: Spatial Data Analysis. John Wiley & Sons, Inc., Hoboken, New Jersey. 695.

Gonzalez, W. D., J. A. Joselyn, Y. Kamide, H. W. Kroehl, G. Rostoker, B. T. Tsurutani, and V. M. Vasyliunas (1994). What is a geomagnetic storm? Journal of Geophysical Research, 99(A4), 5771–5792, https://doi.org/10.1029/93JA02867.

Gonzalez, W.D., Tsurutani, B.T. & Clúa de Gonzalez, A.L. (1999). Interplanetary origin of geomagnetic storms. Space Science Reviews 88, 529–562. https://doi.org/10.1023/A:1005160129098.

GPS WORLD (2024, May 14). How the strong solar storm could impact GNSS. https://www.gpsworld.com/how-the-strong-solar-storm-could-impact-gnss/.

He L, Guo C, Yue Q, Zhang S, Qin Z, Zhang J. A. (2023) Novel Ionospheric Disturbance Index to Evaluate the Global Effect on BeiDou Navigation Satellite System Signal Caused by the Moderate Geomagnetic Storm on May 12, 2021. *Sensors* (Basel). 23(3), 1183. https://doi.org/10.3390/s23031183.

Hofmann-Wellenhof, B., Lichtenegger, H., Wasle, E. (2008) *Global Navigation Satellite System: GPS, GLONASS, GALILEO and more*. Springer Wien New York, , 516p.

Imam, R., Alfonsi, L., Spogli, L., Cesaroni, C., Dovis, F. (2024). On estimating the phase scintillation index using TEC provided by ISM and IGS professional GNSS receivers and machine learning, *Advances in Space Research*. 73(7), 3753-3771 https://doi.org/10.1016/j.asr.2023.07.039.

Komjathy, A. (1997). *Global Ionospheric Total Electron Content Mapping Using the Global Positioning System*. [Ph.D. dissertation, University of New Brunswick]. Report No. 188. https://gge.ext.unb.ca/Pubs/TR188.pdf.

Li, X., Zhang, X., Ren, X., Fritsche M., Wickert, J., Schuh, H. (2015) Precise positioning with current multi-constellation Global Navigation Satellite Systems: GPS, GLONASS, Galileo and BeiDou. Scientific Reports, Nature. 5, 8328; DOI:10.1038/srep08328.

Loewe, C. A., and G. W. Prölss (1997), Classification and mean behavior of magnetic storms, *Journal of Geophysical Research*, 102(A7), 14209–14213, https://doi.org/10.1029/96JA04020.

Lu, Y., Wang, Z., Ji, S., & Chen, W. (2020). Assessing the positioning performance under the effects of strong ionospheric anomalies with multi-GNSS in Hong Kong. *Radio Science*, 55(8), e2019RS007004. https://doi.org/10.1029/2019RS007004.

Luo, X., Gu, S., Lou, Y., Xiong, C., Chen, B., Jin, X. (2018) Assessing the Performance of GPS Precise Point Positioning Under Different Geomagnetic Storm Conditions during Solar Cycle 24. *Sensors*, 18(6), 1784. https://doi.org/10.3390/s18061784.

Luo, X., Du, J., Lou, Y., Gu, S., Yue, X., Liu, J., & Chen, B. (2022a). A method to mitigate the effects of strong geomagnetic storm on GNSS precise point positioning. *Space Weather*, 20(1), e2021SW002908. https://doi.org/10.1029/2021SW002908.

Luo, X., Du, J., Galera Monico, J. F., Xiong, C., Liu, J., & Liang, X. (2022b). ROTI-based stochastic model to improve GNSS precise point positioning under severe geomagnetic storm activity. Space Weather, 20, e2022SW003114. https://doi.org/10.1029/2022SW003114.

Luo, X., Chen, Z., Gu, S., Yue, N.,Yue, T. (2023) Studying the fixing rate of GPS PPP ambiguity resolution under different geomagnetic storm intensities. *Space Weather*, 21 (10), https://doi.org/10.1029/2023SW003542.

Miteva, R., Samwel, S.W. (2023) Catalog of Geomagnetic Storms with Dst Index ≤ −50 nT and Their Solar and Interplanetary Origin (1996–2019). *Atmosphere*, 14(12), 1744. https://doi.org/10.3390/atmos14121744.

Moldwin, M. (2022). *An Introduction to Space Weather* (2nd ed.). Cambridge University Press.

Monico, J. F. G., Dal Poz, A. P., Galo, M., Santos, M. C., Oliveira, L. C. (2009) Acurácia e precisão: revendo os conceitos de forma acurada. *Boletim de Ciências Geodésicas*, 15(3), 469- 483.

Mou Y., Luo X., Xie Z., Peng X. (2023) Performance analysis of four PPP service software under different intensity geomagnetic storms. *Advances in Space Research*, 72(5), 1593-1604. https://doi.org/10.1016/j.asr.2023.04.026.

NASA (National Aeronautics and Space Administration) (2024, May 16) How NASA Tracked the Most Intense Solar Storm in Decades. https://science.nasa.gov/science-research/heliophysics/how-nasa-tracked-the-most-intense-solar-storm-in-decades/.

NOAA (National Oceanic and Atmospheric Administration) (2024a). NOOA Space Weather Scales. https://www.swpc.noaa.gov/noaa-scales-explanation.

NOAA (National Oceanic and Atmospheric Administration) (2024b, May 10). Strong geomagnetic storm reaches Earth, continues through weekend. https://www.noaa.gov/stories/strong-geomagnetic-storm-reaches-earth-continues-through-weekend.

NRCAN (Natural Resources Canada). (2020) CSRS-PPP Version 3: Tutorial. https://webapp.csrs-scrs.nrcan-rncan.gc.ca/geod/tools-outils/sample_doc_filesV3/NRCan%20CSRS-PPP-v3_Tutorial%20EN.pdf.

NRCAN (Natural Resources Canada). (2024a) CSRS-PPP Updates and Information. https://webapp.csrs-scrs.nrcan-rncan.gc.ca/geod/tools-outils/ppp-info.php?locale=en.

NRCAN (Natural Resources Canada). Precise Point Positioning. (2024b) https://webapp.csrs-scrs.nrcan-rncan.gc.ca/geod/tools-outils/ppp.php.

Odolinski, R., Teunissen, P.J.G. (2019) An assessment of smartphone and low-cost multi-GNSS single-frequency RTK positioning for low, medium and high ionospheric disturbance periods. Journal of Geodesy 93, 701–722 https://doi.org/10.1007/s00190-018-1192-5.

Otto, A. *The magnetosphere*. (2005) Part III, Models of Space Weather. In: Scherer, K., Fichtner, H., Heber, B., Mall, U. (Eds.), Space Weather, Lect. Notes Phys. 656 (Springer, Berlin Heidelberg).

Paziewski J, Høeg P, Sieradzki R, Jin Y, Jarmolowski W. (2022). The implications of ionospheric disturbances for precise GNSS positioning in Greenland. *Journal Space Weather Space Climate*. 12 (33). https://doi.org/10.1051/swsc/2022029.

Schunk, R., Nagy, A. (2009) *Ionospheres: Physics, Plasma Physics, and Chemistry*, ISBN: 9780511635342. Cambridge University Press.

SIRGAS. (2024) Weekly XYZ positions sorted by station. https://www.sirgas.org/en/weekly-solutions/xyz_station/.

Space Weather (2024, May 9) What's up in space. https://spaceweather.com/archive.php?view=1&day=09&month=05&year=2024.

Wan, X., Xiong, C., Gao, S. (2021) The nighttime ionospheric response and occurrence of equatorial plasma irregularities during geomagnetic storms: a case study. *Satellite Navigation* 2, 23. https://doi.org/10.1186/s43020-021-00055-x.

Wang, Y.; Yuan, Y.; Li, M.; Zhang, T.; Geng, H.; Wang, G.; Wen, G. (2023) Effects of Strong Geomagnetic Storms on the Ionosphere and Degradation of Precise Point Positioning Accuracy during the 25th Solar Cycle Rising Phase: A Case Study. *Remote Sensing 15*, 5512. https://doi.org/10.3390/rs15235512.

WDC (World Data Center for geomagnetism) (2024). https://wdc.kugi.kyoto-u.ac.jp/dst_realtime/202405/index.html.

Yasyukevich, Y.V., Kiselev, A.V., Zhivetiev, I.V. (2020) SIMuRG: System for Ionosphere Monitoring and Research from GNSS. *GPS Solutions* 24 (69). https://doi.org/10.1007/s10291-020-00983-2.

Zheng Y, Xiong C, Jin Y, Liu D, Oksavik K, et al. (2022). The refractive and diffractive contributions to GPS signal scintillation at high latitudes during the geomagnetic storm on 7–8 September 2017. *Journal Space Weather Space Climate* 12 (40). https://doi.org/10.1051/swsc/2022036.

Zhow, W., Yuan, Y., Tang, C., Meng, Y., Chen, Y. (2024). Ionosphere disturbances on GNSS signal and positioning performance: Analysis of the solar flare and geomagnetic storm events in September 2017 and October 2021. *Advances in Space Research*, 73 (9). e2021SW002908. https://doi.org/10.1016/j.asr.2024.01.044.